In vitro dose measurements in a human cadaver with abdomen/pelvis CT scans

Da Zhang, Atul Padole, Xinhua Li, Sarabjeet Singh, Ranish Deedar Ali Khawaja, and Diego Lira
Department of Radiology, Massachusetts General Hospital, Boston, Massachusetts 02114

Tianyu Liu
Nuclear Engineering Program, Rensselaer Polytechnic Institute, Troy, New York 12180

Jim Q. Shi, Alexi Otrakji, and Mannudeep K. Kalra
Department of Radiology, Massachusetts General Hospital, Boston, Massachusetts 02114

X. George Xu
Nuclear Engineering Program, Rensselaer Polytechnic Institute, Troy, New York 12180

Bob Liu[a)]
Department of Radiology, Massachusetts General Hospital, Boston, Massachusetts 02114

(Received 25 January 2014; revised 29 July 2014; accepted for publication 5 August 2014; published 26 August 2014)

Purpose: To present a study of radiation dose measurements with a human cadaver scanned on a clinical CT scanner.
Methods: Multiple point dose measurements were obtained with high-accuracy Thimble ionization chambers placed inside the stomach, liver, paravertebral gutter, ascending colon, left kidney, and urinary bladder of a human cadaver (183 cm in height and 67.5 kg in weight) whose abdomen/pelvis region was scanned repeatedly with a multidetector row CT. The flat energy response and precision of the dosimeters were verified, and the slight differences in each dosimeter's response were evaluated and corrected to attain high accuracy. In addition, skin doses were measured for radiosensitive organs outside the scanned region with OSL dosimeters: the right eye, thyroid, both nipples, and the right testicle. Three scan protocols were used, which shared most scan parameters but had different kVp and mA settings: 120-kVp automA, 120-kVp 300 mA, and 100-kVp 300 mA. For each protocol three repeated scans were performed.
Results: The tube starting angle (TSA) was found to randomly vary around two major conditions, which caused large fluctuations in the repeated point dose measurements: for the 120-kVp 300 mA protocol this angle changed from approximately 110° to 290°, and caused 8% − 25% difference in the point dose measured at the stomach, liver, colon, and urinary bladder. When the fluctuations of the TSA were small (within 5°), the maximum coefficient of variance was approximately 3.3%. The soft tissue absorbed doses averaged from four locations near the center of the scanned region were 27.2 ± 3.3 and 16.5 ± 2.7 mGy for the 120 and 100-kVp fixed-mA scans, respectively. These values were consistent with the corresponding size specific dose estimates within 4%. The comparison of the per-100-mAs tissue doses from the three protocols revealed that: (1) dose levels at nonsuperficial locations in the TCM scans could not be accurately deduced by simply scaling the fix-mA doses with local mA values; (2) the general power law relationship between dose and kVp varied from location to location, with the power index ranged between 2.7 and 3.5. The averaged dose measurements at both nipples, which were about 0.6 cm outside the prescribed scan region, ranged from 23 to 27 mGy at the left nipple, and varied from 3 to 20 mGy at the right nipple over the three scan protocols. Large fluctuations over repeated scans were also observed, as a combined result of helical scans of large pitch (1.375) and small active areas of the skin dosimeters. In addition, the averaged skin dose fell off drastically with the distance to the nearest boundary of the scanned region.
Conclusions: This study revealed the complexity of CT dose fluctuation and variation with a human cadaver. [http://dx.doi.org/10.1118/1.4893499]

Key words: CT, radiation dosimetry, dose, human cadaver

1. INTRODUCTION

There has been a rising concern about the exposure to ionizing radiation from CT examinations and the associated health risks. One contributing factor to this controversial issue is the difficulty in accurately determining the patient dose from the CT procedure. The validity and accuracy of

the widely used CTDI paradigm has been rigorously re-evaluated,[1,2] and more reliable and clinically relevant dose metrics have been recommended.[3–6] Particularly, American Association of Physicists in Medicine (AAPM) Task Group 204 recommended the size-specific dose estimates (SSDEs), which correct $CTDI_{vol}$ values based on the patient size, and convert $CTDI_{vol}$ into tissue dose estimates at the center of the scanned region (along z).[5,7] In addition, AAPM Task Group 111 developed a new system of CT dose metrics, including the equilibrium dose, midpoint dose, and equilibrium dose-pitch product in phantoms, to circumvent the limitations of CTDI-based metrics. These point-dose based metrics are robust and can represent generic patient-relevant radiation doses accurately in helical and axial CT scans of any beam width and table increment.[6,8]

Although ideal and highly desirable, real-time accurate dose estimation for each patient undergoing CT exams is difficult to achieve due to complexities caused by several factors: (1) patient anatomy and tissue composition;[9] (2) the motion of radiation source(s), table, and the patient; (3) tube current and voltage modulation;[10] (4) the limited dose estimation methods.[11]

CT dose estimation methods are generally based on Monte Carlo simulations and physical measurements. Computational simulations have great versatility in specifying the entire imaging scenario, and have been validated in terms of high accuracy in describing the physical interactions between radiation and material and in calculating energy deposition. However, the flexibility in return requires precise knowledge of the setting of the imaging process (including detailed information of the design of the CT scanner) and significant computational cost.[12] Any deviation of the simulation from the reality will cause errors and biases in the simulated results. Nonetheless, many of the design specifications of commercial CT scanners are proprietary and publicly unavailable, such as bowtie filters and other intrinsic filtration materials. The lack of such key information made many researchers in the field of CT dose simulation resort to experimental estimation approaches for the equivalent shape and composition of bowtie filters.[13,14] Computational phantoms employed in the simulation are also critical for accurate dose simulation. These phantoms have evolved from the stylized phantoms (with simple shapes and compositions) to voxelized phantoms,[9,15] and to more advanced mesh based phantoms.[16–19] A comprehensive review on the development of computational phantoms for radiation dosimetry can be found in Ref. 9. With the advances in both computational phantoms and modeling of CT systems, several research groups have worked on more patient-specific CT dose estimation methods.[20–26] One such software is the VirtualDose (www.virtual-dose.com) that employs a library of adult and pediatric patient phantoms for organ dose reporting.

On the other hand, physical measurements of CT dose are based on the exact scanner and the imaging setup, and are often used as benchmarks to validate the more convenient Monte Carlo simulations.[20,27,28] Experimental measurements are however subject to imperfections of radiation measurement systems.[29] For example, energy-dependent gain calibration is necessary to interpret direct dose readings from dosimeters, such as optically stimulated luminescence dosimeters (OSLD), thermal luminescence dosimeters (TLD), and MOSFET detectors.[30–32] Such interpretation is difficult since the beam quality inside the scanned volume cannot be easily quantified experimentally.[33] In addition, the measurement results can also be influenced by dosimeter characteristics including reproducibility, gain uniformity across multiple detectors, and angular dependence (dependence on the direction of incident beams).[30,31,34,35] Another limitation of physical measurements is that dose measurements are often made inside phantoms or in air, as it is extremely difficult to perform direct dose measurements inside human subjects.[9] To acquire a reliable *in vitro* data set of radiation dose in a human subject, efforts are needed in the selection and characterization of dosimeters, experimental design and control, and data processing. Nevertheless, human subjects are the ideal targets for radiation dosimetry studies and the ultimate benchmarks for validating dose simulation methods. In recent scientific conferences a few groups reported preliminary results in this direction: a group of researchers performed multiple CT organ dose measurements with cadavers of different body mass index (BMI), and their measurements were based on OSLDs contained by sealed tubes partially inserted inside the cadavers;[36,37] another group of researchers performed *in vivo* dose measurements with TLDs affixed to the inner lumen of rectal catheters for multiple patients undergoing CT Colonography.[38]

This paper describes an experimental dose measurement study performed using a human cadaver, in which multiple point dose measurements were obtained with high-accuracy dosimeters placed inside the stomach, liver, paravertebral gutter, ascending colon, left kidney, and urinary bladder of the human cadaver whose abdomen/pelvis region was scanned repeatedly with multiple CT protocols. To our knowledge, there are no prior published data of this kind in the literature. In addition, skin doses were measured for radiosensitive organs outside the scanned region: the right eye, thyroid, both nipples, and the right testicle. The purpose of the study was threefold: (a) to conduct point dose measurements inside/near radiosensitive organs with a real human subject using clinical scanning protocols; (b) to examine how these dose measurements vary with different scanning conditions; and (c) to provide a benchmark dataset for the development, validation, and refining of Monte Carlo dose simulation programs.

2. MATERIALS AND METHODS

2.A. Cadaver acquisition and handling

This study was approved by the internal review board of the institution (Massachusetts General Hospital) where the experiments were performed. The cadaver, acquired from a nonprofit and accredited entity, Science Care (Phoenix, AZ), was an 88 years old white male, 183 cm in height and 67.5 kg in weight, who died from natural causes (more details listed in Table I). The cadaver was thawed for three days af-

TABLE I. Body habitus of the human cadaver. The AP and LAT diameters were measured near the center of the scanned region, approximately at the slice of the thimble ion chamber in the colon in Fig. 1.

Age (yr)	Gender	Height (cm)	Weight (kg)	BMI (kg/m^2)	AP diam. (cm)	LAT diam. (cm)
88	Male	183	67.5	20.2	33.2	20.4

ter its arrival at the hospital, and then the dose experiments were performed (within two weeks from the date of death). The cadaver was shipped back to Science Care after the experiments.

2.B. Characterization and calibration of dosimeters inside the cadaver

The point dose measurements inside internal organs involved placement of multiple Thimble chambers (Model 10x5-0.6CT and 10x6-0.6CT, Radcal Inc., Monrovia, CA). These chambers have an active length of 21 mm and an active volume of 0.6 cm^3, and have very small exposure rate dependency ($\pm 2\%$ over $10 - 100R/s$) and almost flat response with about 1.5% variation over half value layers (HVL) between 2 and 15 mm of Aluminum.[6] The two models of the Thimble chambers share the same chamber design but have different interfaces for connecting to various dose monitors. In addition, the 10x6-0.6CT model has a built-in temperature sensor in the chamber, which helped determine the internal temperature of the cadaver for the dose calibration purpose. Each chamber was assigned to a compatible dose monitor (Models Accu-Gold, 9010, 9015, and 9095, Radcal Inc., Monrovia, CA) and formed altogether six dosimeter systems. A cross-system calibration was performed to address the potential problem of bias caused by the differences in each systems' response.

One of the six dosimeter systems, whose calibration was traceable to National Institute of Standards and Technology (NIST), was chosen as the reference system for the cross calibration. During the calibration, the chamber was placed in the central and peripheral (12 o'clock) holes of a 32-cm CTDI phantom, and its charge collection volume was centered at the phantom's central plane with phantom adapters (Model 8430CT, Radcal Inc., Monrovia, CA). The phantom adapters filled the rest part of the hole with the same phantom material. The phantom was placed at the isocenter of the CT scanner (GE LightSpeed 16 Pro, Waukesha, WI) used for the cadaver study, and was irradiated by an axial scan with 20-mm beam collimation width and body bowtie filter in each measurement. To reduce quantum noise, large exposures at 640 mAs were used. Three repeated measurements were made for each position and for each available kVp (80, 100, 120, and 140), and the service mode of the scanner was used for the precise control of the scanning. The same measurements were repeated for the other five dosimeter systems.

The weighted average of the central and peripheral position measurements was calculated according to $D_w = 1/3 \times \overline{D_c} + 2/3 \times \overline{D_p}$. The D_w was then used to calculate the cross-system calibration factor,

$$f_{sys}(kVp) = \frac{D_{w,i}(kVp)}{D_{w,ref}(kVp)}, \quad (1)$$

where $D_{w,i}$ is the weighted average dose value for the ith dosimeter system.

During the cross-system calibration of the Thimble chamber systems, we verified that the response of the systems were insensitive to the beam quality. In addition, for each Thimble chamber system, all measurements were repeatable under identical conditions with coefficients of variance (COV) within 0.5%.

2.C. Positions of the dosimeters

The following surgical procedure for placing the dosimeters were performed by the radiologists and interventional radiologists of the co-authors. Midline vertical and horizontal incisions were made in the anterior abdominal wall from xiphoid process to the pubic symphysis pubis. Four Thimble chambers were embedded inside the following organs of the abdomen/pelvis part of the subject: stomach, liver, ascending colon, and urinary bladder. Another chamber was glued to the anterior surface of the left kidney and the remaining chamber was sutured and glued to the left psoas muscle adjacent to the small intestine in the left paravertebral region. These chambers were covered with thin rubber sheaths for protection against liquids inside the cadaver. The Thimble chambers and cables were secured in respective positions using surgical sutures, surgical glue, and tape. The surgical procedure was performed in the morgue of our hospital, where all autopsy procedures are performed.

The temperature inside the cadaver were monitored by the built-in sensors on the 10x6-0.6CT chambers (24 °C), and was very close to the room temperature in the scan room. The gas law corrections were performed based on the temperature and pressure detected by the dosimeter systems.[39]

Besides the Thimble chambers, five OSLDs were placed on the skin outside the scanned region for the right eye, thyroid, both nipples, and the right testicle for each scan.

After the surgical procedure to place the Thimble chambers, a whole-body scan of the cadaver was performed to verify the positions of the dosimeters and to provide a complete image database for postprocessing and analysis.

Figure 1 shows the placement of the Thimble chambers. The central image in Fig. 1 was generated by a slice-rendering in the AP direction, and shows the overall positioning of the Thimble chambers in the coronal plane. Because the chambers were embedded at different depths, only the chamber at the stomach was visible in this coronal slice. The axial

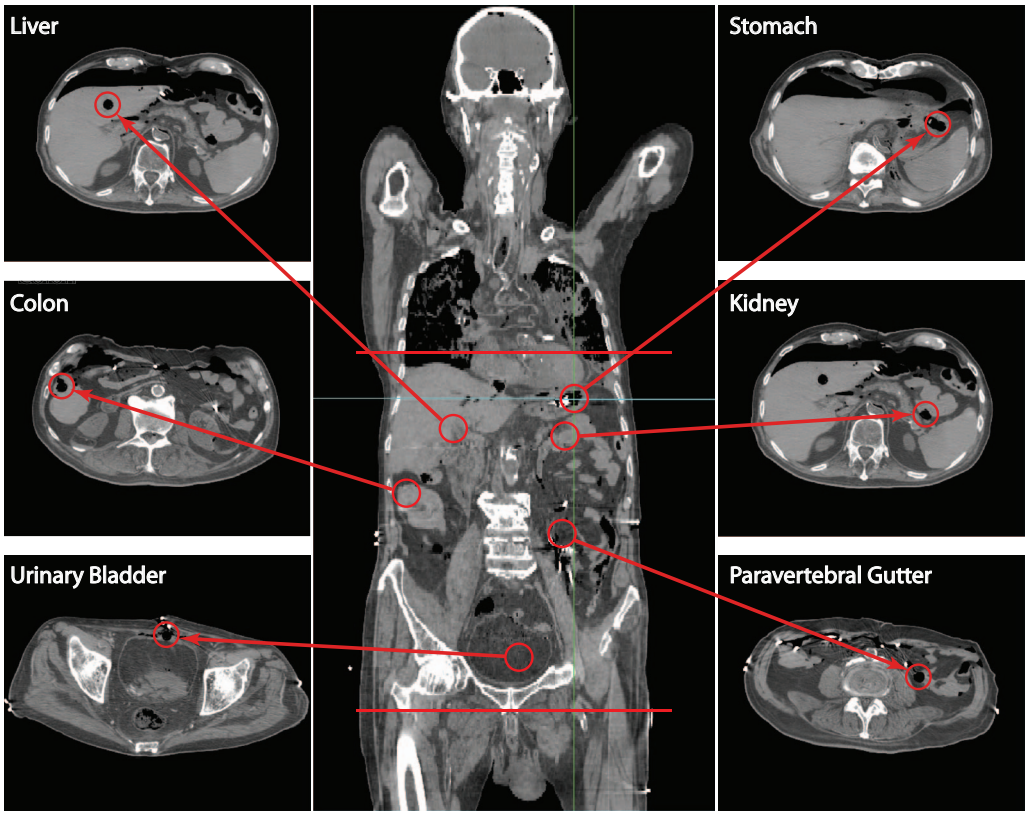

FIG. 1. Coronal multiplanar reformat and transverse images depicting the locations of the Thimble chambers inside the abdomen and pelvis region of the cadaver for dose measurements in the stomach, liver, left kidney, ascending colon, paravertebral region, and urinary bladder.

images containing the active volume of each chamber (a black cavity filled by air) are shown on both sides of the coronal view.

2.D. Scanning setup

A mutlidetector-row CT scanner (GE LightSpeed 16 Pro, GE Healthcare, Waukesha, WI) was used for scanning the cadaver following placement of the dosimeters. For scanning, the human cadaver was placed in a supine position on the CT table. The arms were raised above the head as per routine clinical practice in live human subjects undergoing CT. The cadaver was centered in both x and y axes, and the optimal centering was confirmed by two radiologists prior to the scanning. The cadaver was not moved relative to the CT table during the entire scanning.

Three scan protocols were selected to scan the abdomen/pelvis region of the subject: (1) 120 kVp with longitudinal tube current modulation (TCM); (2) 120 kVp with fixed mA; and (3) 100 kVp with fixed mA. The scanning parameters of these protocols are listed in Table II. For each protocol, three repeated scans were performed.

The 120-kVp automA protocol was modified from the clinical routine adult abdomen/pelvis protocol at the hospital: the rotation time was changed from 0.5 to 1 s, and only longitudinal TCM (automA) with the widest mA range (10–670) was used. These modifications were made to reduce the statistical error from photon fluctuation by increasing the radiation levels, and to lower the complexity of the scan dataset by avoiding the x-y plane TCM, for the ease of post processing. The fixed mA protocols were modified from the TCM protocol to study the influence of TCM and different tube voltages. The tube current values were obtained from the DICOM images for the 120-kV automA protocol, and the mA curve was overlaid on top of the lateral-view of the subject in Fig. 2. The start and the end of the scanned region were marked previously in Fig. 1.

TABLE II. Scan parameters for the three protocols. (Key: "SFOV": scan field of view, "Rot. Time": rotation time, "Beam Coll.": beam collimation). The reported $CTDI_{vol}$ for the fixed mA protocols were measured on the scanner. The 120-kVp fixed mA result was scaled by the average mA of the TCM protocol to obtain its $CTDI_{vol}$.

Protocol	kVp	Tube current (mA)	Rot. Time (s)	Pitch	Beam colli . (mm)	SFOV	Bowtie	Noise index	$CTDI_{vol}$ (mGy)
1	120	TCM	1.0	1.375:1	16 × 1.25	Large	Body	15	26.6
2	120	300	1.0	1.375:1	16 × 1.25	Large	Body	NA	18.3
3	100	300	1.0	1.375:1	16 × 1.25	Large	Body	NA	11.5

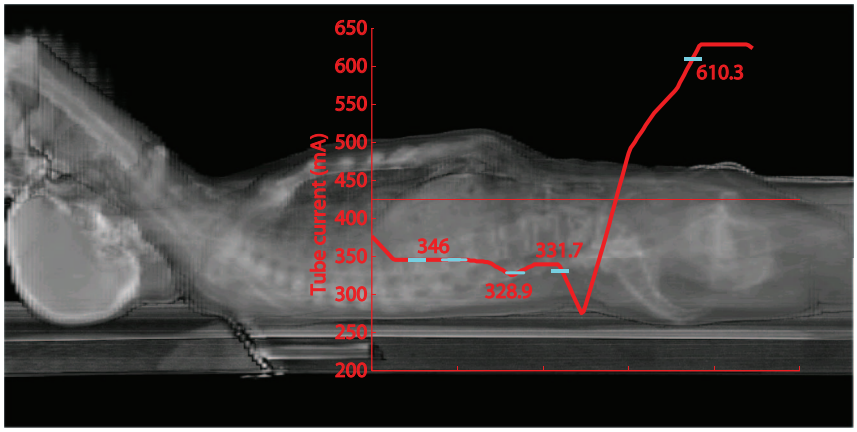

FIG. 2. The lateral view of the subject with tube current modulation overlaid on top it. The averaged mA values near the Thimble chambers (±10 mm around the center of the active volumes of the chambers) are labeled on the tube current curve.

2.E. Processing of OSLD measurements

Five new OSLDs were used for each repeated scan. These OSLDs were read twice to reduce the read-out fluctuation, and the background readings were subtracted from the average of the two readings.[40] For both nipples which were close to the boundary of the scanned region, the beam quality was considered the same as the primary beam because of overscan.[41] For the other three locations of the OSLDs, we adopted the conservative estimation that the scattered rays had the same beam qualities as the primary beams.[42] The dose measurements (air kerma) were corrected by the respective energy dependent calibration factors, and were converted to soft tissue absorbed doses using a conversion factor of 1.073 mGy/mGy.[5] The calibration procedure of OSLDs was detailed in a previous study which reported a method for obtaining densely sampled dose maps inside an anthropomorphic phantom with OSLDs.[40]

3. RESULTS

3.A. Dose measurements at internal organs

Figure 3 showed the cross-system calibration factors of all the six Thimble chamber systems, with dosimeter system #3 being the reference system (the calibration factors for this system are one for all the kVp settings). The response varied from system to system, with the highest deviation below 0.05, and most of the deviations within 0.02. It should also be noted that the variation due to different kVp was below 0.005, showing the flat energy response of the Thimble chamber systems.

The direct Thimble chamber readings (in Roentgen) were corrected by dividing them with the respective cross-system calibration factors. These exposure levels were then converted to soft-tissue absorbed dose (hereafter referred to as "tissue dose") using an f-factor of 9.37 mGy/R.[5]

The individual dose measurements were plotted in Fig. 4, and the three repeated measurements were separated horizontally: the first on the left, the second at the center, and the third on the right. The mean and standard deviation (SD) from the repeated measurements were calculated for each chamber position and for each scanning protocol. Some large variations

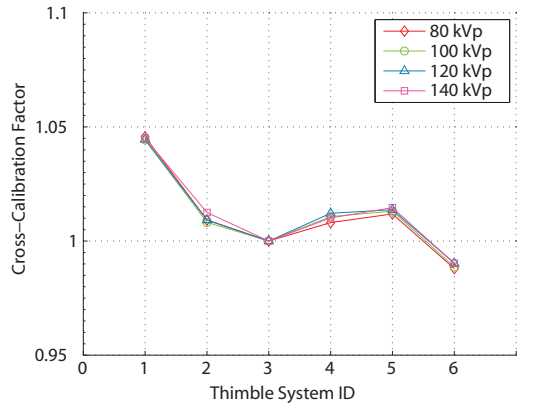

FIG. 3. Cross-system calibration factors of six Thimble chamber systems.

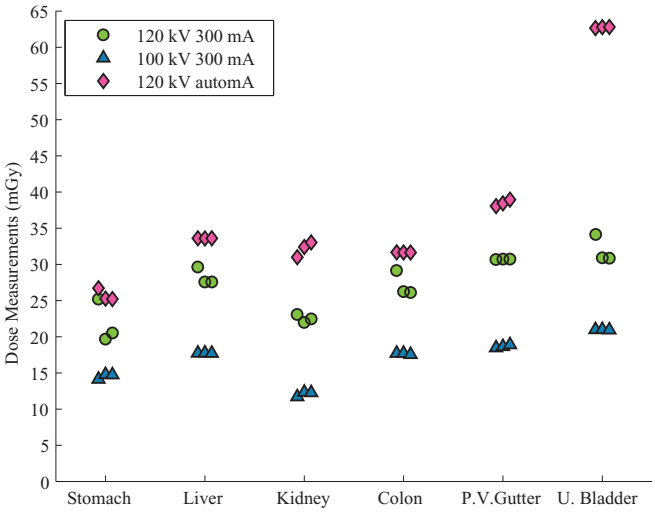

FIG. 4. Scatter plot of the dose measurements inside the cadaver's abdomen/pelvis region. For each protocol and each organ, three data points were shown. These data points were slightly shifted in the horizontal direction to represent repeated measurements: the first on the left, the second at center, and the third on the right.

TABLE III. Soft tissue absorbed dose per 100 mAs sampled by the Thimble chambers, grouped by scan protocols and tube starting angles (TSA). The TSA of the repeated scans were listed at the end of each row, following the order of the scans. Due to the large differences in TSA of the 120-kVp fixed-mA scans, the first scan of this protocol was separated from the other two repeated scans for the analysis. Averaged tissue dose values and the corresponding COVs were calculated for each group (excluding the first repeat of the 120-kVp fixed-mA protocol). The tissue dose in the automA scans were normalized based on local mAs values, which were 346, 346, 346, 328.9, 331.7, and 610.3 mA for the chambers near the stomach, liver, left kidney, ascending colon, paravertebral gutter, and urinary bladder, respectively.

Avg. tissue dose (mGy)	Stomach	Liver	L. Kidney	Colon	P. V. Gutter	U. Bladder	TSA (°)
120-kVp automA, repeat 1-3	7.43	9.71	9.29	9.62	11.60	10.28	106.8, 108.3, 109.0
COV	3.31%	0.04%	3.24%	0.05%	1.15%	0.14%	
120-kVp fixed-mA, repeat 1	8.40	9.89	7.69	9.72	10.22	11.38	290.0
120-kVp fixed-mA, repeat 2-3	6.70	9.19	7.41	8.72	10.25	10.30	109.6, 114.3
COV	2.93%	0.00%	1.66%	0.31%	0.04%	0.04%	
100-kVp fixed-mA, repeat 1-3	4.85	5.91	4.03	5.88	6.22	6.99	294.8, 294.1, 293.0
COV	2.55%	0.08%	2.92%	0.53%	1.18%	0.13%	

were observed from the 120-kVp fixed-mA protocol: COVs of the point dose measurements at the stomach, liver, colon, and urinary bladder were 13.7%, 4.2%, 6.4%, and 5.9%, respectively. The maximum COV for all other points in Fig. 4 was about 3.3%.

From the DICOM images, the "Trigger On Position" were extracted to carefully investigate the tube starting angle, which was assumed to be the main contributing factor in the large fluctuations as seen in Fig. 4. According to the DICOM conformance statement of the scanner, this DICOM field refers to the angular position where data acquisition starts. The tube starting angles listed in Table III shows that the tube started from two major stations (with variations), one near 290° and the other near 110° (0° represents the 12 o'clock position). More importantly, the large difference of approximate 180° between the first and the rest two scans of the 120-kVp fixed-mA protocol was found to cause considerable difference in the doses sampled at the stomach, liver, colon, and urinary bladder, leading to the large fluctuation mentioned in the previous paragraph.

The averaged tissue dose values at different locations ranged from 25.7 to 62.7 mGy (with a six-location average of 37.4 mGy) in the 120-kV TCM scan, from 21.8 to 32.0 mGy (averaged 27.1 mGy) in the 120-kV fixed-mA scan, and from 12.1 to 21.0 mGy (averaged 16.9 mGy) in the 100-kV fixed-mA scan. The effective diameter of the cadaver in the abdomen/pelvis region was approximately 26 cm (calculated using the $\sqrt{AP \times LAT}$ formula[5]), and SSDEs were calculated from the $CTDI_{vol}$ to be 26.2 and 16.4 mGy for the 120- and 100-kVp fixed-mA scans, respectively. To compare with the SSDEs values, averaged tissue doses were calculated from the four locations near the center of the scanned region in the longitudinal direction (liver, paravertebral gutter, kidney, and colon). The radial distances from these chambers to their cross-sectional centers of the scanned volume were 5.1, 7.3, 12.8, and 7.0 cm, respectively.

These four-location averaged tissue doses were 27.2 mGy (SD: 3.3 mGy) and 16.5 mGy (SD: 2.7 mGy) for the 120- and 100-kVp fixed-mA protocols, and were slightly differed from the respective SSDEs by 4% and 1%.

The tissue dose per 100 mAs was calculated and presented in Table III. For the fixed-mA scans, the tissue dose values were normalized to 100 mAs. For the automA scans, the local mAs values were used for the normalization. The tube currents near the active volumes of the chambers (±10 mm, covering the width of the direct beam and the length of the active volumes) were averaged, and the results were 346, 346, 346, 328.9, 331.7, and 610.3 mA for the chambers near the stomach, liver, left kidney, colon, paravertebral gutter, and urinary bladder, respectively. These local mA values are labeled in Fig. 2.

In Table III, relative differences between the normalized tissue dose values from the three scans of the 120-kVp automA scans and those from the last two repeated scans of the 120-kVp fixed-mA protocol were 11.0%, 5.7%, 25.4%, 10.4%, 13.2%, and −0.2% for the stomach, liver, left kidney, colon, paravertebral gutter, and urinary bladder, respectively.

The kVp dependency of radiation doses was tested by plotting the ratios between the dose levels in the 100-kVp scans and the 120-kVp fixed-mA scans in Fig. 5. The horizontal dashed line indicated the ratio between the average doses from all the six locations. These ratios were converted into $(100/120)^{power}$ for testing the known power law relationship between dose and kVp.[41] Measurements from only the first

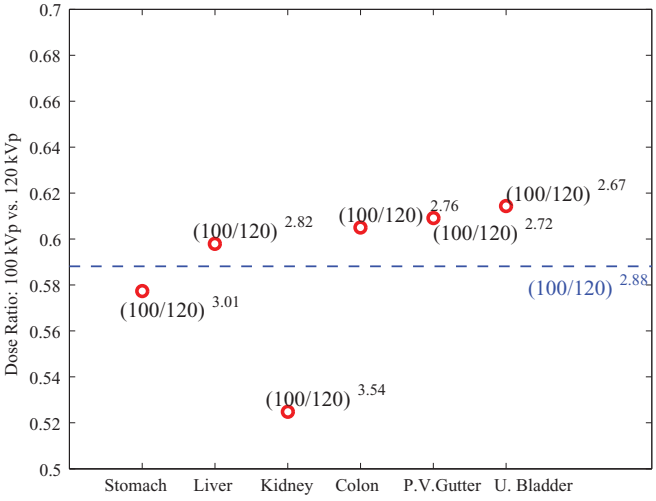

FIG. 5. Ratio between the doses in the 100 and 120-kVp fixed mA scans. These ratios were converted into $(100/120)^{power}$.

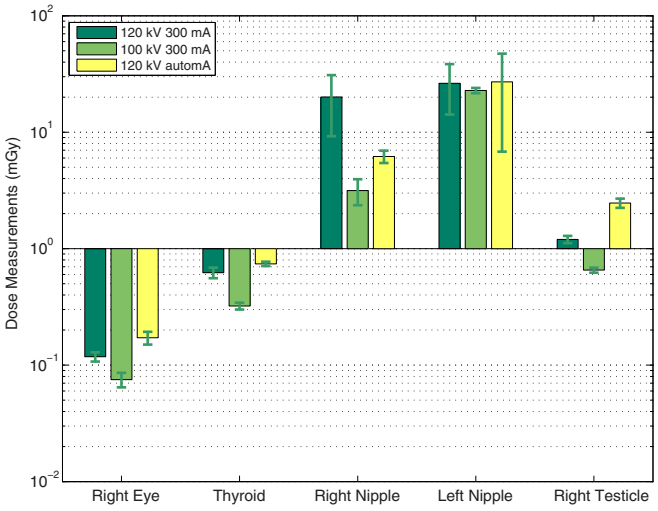

FIG. 6. OSLD Skin dose measurements at five locations outside the scanned region. The error bars represent the standard deviations from the repeated measurements, which appeared asymmetric in log scale.

repeat for the 120-kVp fixed-mA protocol were used to eliminate the influence of the large difference in the tube starting angles.

3.B. Skin dose measurements outside the scan region

The skin dose measurements were plotted in log scale in Fig. 6. At both nipples which were about 0.6 cm outside the boundary of the scan region, large dose levels were observed: the averaged doses ranged from 23 to 27 mGy at the left nipple and varied from 3 to 20 mGy at the right nipple over the three protocols. The large fluctuations over repeated scans could be attributed to that the nipples were covered by the primary beam due to overscan (estimated as 1.5 cm on each end of the scanned range in z).[41] In Fig. 7, the averaged skin dose fell off drastically with the distance from the OSLDs to the nearest boundary of the scanned region. One should note the dose measurements at the eye had magnitudes close to the background signals (0.1–0.2 mGy), and their accuracy may be affected by readout errors.[34]

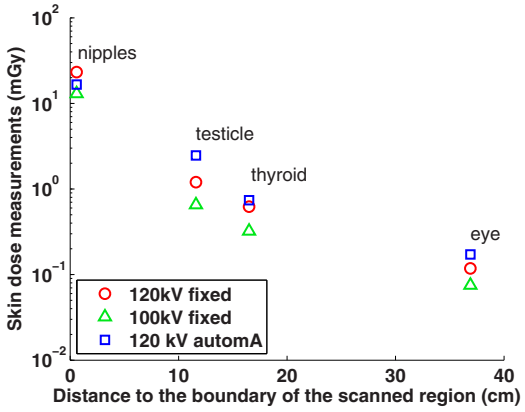

FIG. 7. Skin dose levels against the distance to the nearest boundary of the scan region.

4. DISCUSSION AND CONCLUSION

One of the main purposes of this experiment was to acquire a reliable dose data set from a human cadaver undergoing CT scans. To that end, we specified several requirements for the dosimeters used inside the cadaver: (1) the dosimeters should be compact for point measurements; (2) they need to be visible in CT images for visually verifying their placement; (3) they should be repeatedly readable after their placement is fixed; (4) their response should not have strong dependency on the beam quality, exposure rate, and direction of incident beam from rotating x-ray source; (5) the difference in the response across multiple dosimeter systems should be small; (6) they should have high precision (low fluctuation). After carefully reviewing and experimentally evaluating a few candidate dosimetry systems including MOSFET dosimeters, OSLDs, and Thimble ionization chamber based dosimeters, we decided to use Thimble chambers as the dosimeters for measuring dose inside the cadaver. During the cross-system calibration process, we verified the high precision and stable responses of these systems. By the careful experimental design and preparation, we managed to minimize the uncertainties from the measuring techniques and experimental setups, and revealed the complexities of dose distribution in realistic CT scans with real human subjects.

The dimension of the cadaver is much smaller than that of the 32-cm diameter CTDI phantom. As a result, the tissue dose levels sampled at the internal organs were larger than the $CTDI_{vol}$ (converted to tissue dose with the f-factor of 1.073 mGy/mGy) by 31%–38%. SSDE, which is a patient dose estimate that employs corrections based on the size of the patient, is exactly designed to address the above differences.

Since SSDE estimates the averaged tissue dose at the center of the scanned region (along z), we compared the SSDE values with the tissue doses averaged from four locations near the center of the scanned volume (Sec. 3.A). These four-location averaged tissue doses in the two fixed-mA protocols agreed well with the SSDEs within 4%.

We made three repeated scans for each protocol to evaluate the fluctuation in the data. Although most of the data points in Fig. 4 have relatively small fluctuations (max COV ≈3.3%), larger variations occurred at the stomach, liver, colon, and urinary bladder in the 120-kVp fixed-mA scans. We noted that these locations were shallower in the axial plane than the other two locations (Fig. 1): the chambers at the colon and the bladder were close to the surface of the cadaver, and all the four chambers were near air-filled cavities (natural or introduced by the surgical procedure). In addition, we used a pitch factor of 1.375 in all the scans. This large pitch caused gaps between the x-ray beams from consecutive rotations of the x-ray source, and made the positions of the helices dependent on the starting angle of the x-ray tube. Dramatic dose variation near the periphery of a scanned volume, which was caused by different tube starting angles alone, has also been reported in the literature.[22,23,43] This characteristic of the helical CT scans created a random factor into our point dose measurements.

When we further investigated the scatterness of the individual measurements in Fig. 4, we found that at each location

and for each scan protocol, there were at most two well separated dose levels. This stimulated us to examine the tube starting angles. We found that the tube starting angles could randomly change between two well separated conditions which were approximately 180° apart, and small variations occurred under each condition (Table III). The large change in the tube starting angles in the 120-kVp fixed-mA scans correlated well with the variation in the dose measurements.

To calculate per-100-mAs tissue dose values (Table III) for the automA scans, we used mA averaged from ±10 mm of the active volumes of the chambers. The reason for using these locally averaged mA values in the normalization was: (1) the chamber at the urinary bladder, where the tube current raised above 600 mA, was near the skin of the cadaver where primary x-rays dominated the dose measurements; (2) these mA values only varied slightly at other five locations (Fig. 2).

The 120-kVp automA scans and the last two repeats of the 120-kVp fixed-mA scans shared similar tube starting angles (≈110°), and the comparison of these two groups in Table III provided some insights about the influence of the longitudinal TCM: at the superficial chamber location near the urinary bladder, the tissue dose values after normalization were almost identical; the relative difference were larger at deeper locations such as the left kidney (25.4%) and the paravertebral gutter (13.2%). Two chambers were placed at approximately the same axial plane for the liver and the left kidney. In the 120-kVp automA scans, the averaged normalized tissue dose at the liver was 24% higher than that at the left kidney, whereas these two values differed by less than 5% in the 120-kVp fixed-mA scans. From the above analysis, one can see that TCM profoundly changed the dose distribution inside the scanned volume, and dose levels at nonsuperficial locations in the TCM scan could not be accurately deduced by simply scaling the fix-mA doses with local mA values. Radiation doses in CT are contributed by scattered x-rays significantly, and deeper locations receive scattered photons from locations further away in the longitudinal directions.

We also tested the power law between the radiation dose and kVp, which assumes that the radiation dose is proportional to $(kVp)^{\text{power}}$. The parameter "power" is known to be approximately 2.5 for CT applications.[41] In Fig. 5, the power varied from organ to organ in the approximate range between 2.7 and 3.5. This observation demonstrated again the complexity of CT dose in human subjects from realistic scans.

The abdomen/pelvis scans in this study was prescribed from the dome of liver to symphysis pubis, which was consistent with our clinical adult routine abdomen/pelvis protocol. The nipples of this subject happened to be close to but not covered in this region. Nevertheless, large radiation levels were still observed at these locations (Fig. 6). Due to the variations in tube starting angle and the displacements of the helices in the z-direction, drastic dose variations were observed at the nipples. In Fig. 6, one can see that the two spots had different dose levels despite that they were in the same axial plane and were scanned with the same protocol. This was the combined result of helical scans with large pitch, as well as small active areas of the OSLDs (3 mm in diameter). The drastic fall-off of the mean skin dose readings with distance from the boundary of the scan region in Fig. 7 met our expectations.

There are limitations in this study. The Thimble ion chamber measurements were point dose measurements, and the number of these dose samples was limited by the number of available Thimble ion chambers and dose monitors, and by the time and difficulties of placing the chambers securely inside the cadaver. The point dose measurements should not be confused with organ doses that estimate average dose across the entire organ volume. In contrast to the high sensitivity of the dose samples in this study (Table III), the organ dose uncertainty due to random tube starting angle was reported to be less than 10% for most organs in a recent Monte Carlo based dose simulation study.[23] Only one cadaver (with BMI of 20 kg/m^2) was available at the time of this study, which limited us from exploring the influence of different body habitus. Although the SSDE values agreed well with the four-point average doses in this study, the same level of agreement may not be achievable for subjects with higher BMI. SSDE estimates the dose averaged over the central section of the scanned volume, whereas for obese patients the organs are more centrally located and average dose sampled at radiosensitive inner organs may be lower than the SSDE values.[44] The tube currents for calculating per-100-mAs dose values were retrieved retrospectively from DICOM headers, which may differ from the actual mA profile used during scanning. The OSLDs placed on the skin for the eye, thyroid, and testicle were far from the scanned region, and they received scattered radiation from different directions. The angular dependency of the OSLDs might influence the accuracy of their measurements.

In conclusion, an experimental CT dose study with a human cadaver was presented in this paper. Using six high-accuracy dosimeters and with careful experiment design, the complexity of dose fluctuation and variation was investigated in detail. The data set generated in this study are being used for the development, validation, and refining of Monte Carlo dose simulation programs.[45]

ACKNOWLEDGMENTS

This research is sponsored in part by the National Institute of Biomedical Imaging and Bioengineering (R01EB015478). The authors want to acknowledge Dr. Paul Fitzgerald from GE Global Research and Dr. Paavana Sainath and Dr. Grant Stevens of GE Healthcare for their valuable assistance in the investigation about the tube starting angles.

[a]Author to whom correspondence should be addressed. Electronic mail: bliu7@mgh.harvard.edu

[1]R. L. Dixon, "A new look at CT dose measurement: Beyond CTDI," Med. Phys. **30**, 1272–1280 (2003).
[2]C. H. McCollough, S. Leng, L. Yu, D. D. Cody, J. M. Boone, and M. F. McNitt-Gray, "CT dose index and patient dose: They are not the same thing," Radiology **259**, 311–316 (2011).
[3]R. L. Dixon and A. C. Ballard, "Experimental validation of a versatile system of CT dosimetry using a conventional ion chamber: Beyond CTDI 100," Med. Phys. **34**, 3399–3413 (2007).
[4]X. Li, D. Zhang, and B. Liu, "Monte Carlo assessment of CT dose equilibration in PMMA and water cylinders with diameters from 6 to 55 cm," Med. Phys. **40**, 031903 (10pp.) (2013).

[5]AAPM Task Group 204, *Size-Specific Dose Estimates (SSDE) in Pediatric and Adult Body CT Examinations: Report of AAPM Task Group 204* (American Association of Physicists in Medicine, College Park, MD, 2011).
[6]AAPM Task Group 111, *Comprehensive Methodology for the Evaluation of Radiation Dose in X-Ray Computed Tomography* (American Association of Physicists in Medicine, College Park, MD, 2010).
[7]J. A. Brink and R. L. Morin, "Size-specific dose estimation for CT: How should it be used and what does it mean?" Radiology **265**, 666–668 (2012).
[8]X. Li, D. Zhang, and B. Liu, "Calculations of two new dose metrics proposed by AAPM task group 111 using the measurements with standard CT dosimetry phantoms," Med. Phys. **40**, 081914 (8pp.) (2013).
[9]*Handbook of Anatomical Models for Radiation Dosimetry*, edited by X. G. Xu and K. F. Eckerman (Taylor and Francis, New York, 2009).
[10]R. L. Dixon and J. M. Boone, "Dose equations for tube current modulation in CT scanning and the interpretation of the associated CTDIvol," Med. Phys. **40**, 111920 (14pp.) (2013).
[11]W. Huda, E. L. Nickoloff, and J. M. Boone, "Overview of patient dosimetry in diagnostic radiology in the usa for the past 50 years," Med. Phys. **35**, 5713–5728 (2008).
[12]M. Ljungberg, S.-E. Strand, and M. A. King, *Monte Carlo Calculations in Nuclear Medicine—Applications in Diagnostic Imaging*, 2nd ed. (CRC Press, New York, 2013).
[13]J. M. Boone, "Method for evaluating bow tie filter angle-dependent attenuation in CT: Theory and simulation results," Med. Phys. **37**, 40–48 (2010).
[14]A. C. Turner, D. Zhang, H. J. Kim, J. J. DeMarco, C. H. Cagnon, E. Angel, D. D. Cody, D. M. Stevens, A. N. Primak, C. H. McCollough, and M. F. McNitt-Gray, "A method to generate equivalent energy spectra and filtration models based on measurement for multidetector CT Monte Carlo dosimetry simulations," Med. Phys. **36**, 2154–2164 (2009).
[15]C. Lee, J. L. Williams, C. Lee, and W. E. Bolch, "The UF series of tomographic computational phantoms of pediatric patients," Med. Phys. **32**, 3537–3548 (2005).
[16]X. G. Xu, V. Taranenko, J. Zhang, and C. Shi, "A boundary-representation method for designing whole-body radiation dosimetry models: Pregnant females at the ends of three gestational periods – RPI-P3, -P6, and -P9," Phys. Med. Biol. **52**, 7023–7044 (2007).
[17]W. P. Segars, G. Sturgeon, S. Mendonca, J. Grimes, and B. M. W. Tsui, "4D XCAT phantom for multimodality imaging research," Med. Phys. **37**, 4902–4915 (2010).
[18]Y. H. Na, B. Zhang, J. Zhang, P. F. Caracappa, and X. G. Xu, "Deformable adult human phantoms for radiation protection dosimetry: Anthropometric data representing size distributions of adult worker populations and software algorithms," Phys. Med. Biol. **55**, 3789–3811 (2010).
[19]Y. Zhang, X. Li, W. Paul Segars, and E. Samei, "Organ doses, effective doses, and risk indices in adult CT: Comparison of four types of reference phantoms across different examination protocols," Med. Phys. **39**, 3404–3423 (2012).
[20]G. Jarry, J. J. DeMarco, U. Beifuss, C. H. Cagnon, and M. F. McNitt-Gray, "A Monte Carlo-based method to estimate radiation dose from spiral CT: From phantom testing to patient-specific models," Phys. Med. Biol. **48**, 2645–2633 (2003).
[21]A. C. Turner, M. Zankl, J. J. DeMarco, C. H. Cagnon, D. Zhang, E. Angel, D. D. Cody, D. M. Stevens, C. H. McCollough, and M. F. McNitt-Gray, "The feasibility of a scanner-independent technique to estimate organ dose from MDCT scans: Using ctdivol to account for differences between scanners," Med. Phys. **37**, 1816–1825 (2010).
[22]X. Li, E. Samei, W. P. Segars, G. M. Sturgeon, J. G. Colsher, G. Toncheva, T. T. Yoshizumi, and D. P. Frush, "Patient-specific radiation dose and cancer risk estimation in CT: Part I. Development and validation of a Monte Carlo program," Med. Phys. **38**, 397–407 (2011).
[23]X. Li, E. Samei, W. P. Segars, G. M. Sturgeon, J. G. Colsher, G. Toncheva, T. T. Yoshizumi, and D. P. Frush, "Patient-specific radiation dose and cancer risk estimation in CT: Part II. Application to patients," Med. Phys. **38**, 408–419 (2011).
[24]C. Lee, K. P. Kim, D. Long, R. Fisher, C. Tien, S. L. Simon, A. Bouville, and W. E. Bolch, "Organ doses for reference adult male and female undergoing computed tomography estimated by Monte Carlo simulations," Med. Phys. **38**, 1196–1206 (2011).
[25]C. Lee, K. P. Kim, D. J. Long, and W. E. Bolch, "Organ doses for reference pediatric and adolescent patients undergoing computed tomography estimated by Monte Carlo simulation," Med. Phys. **39**, 2129–2146 (2012).
[26]X. Tian, X. Li, W. P. Segars, D. P. Frush, E. K. Paulson, and E. Samei, "Dose coefficients in pediatric and adult abdominopelvic CT based on 100 patient models," Phys. Med. Biol. **58**, 8755–8768 (2013).
[27]P. Deak, M. Straten, P. Shrimpton, M. Zankl, and W. A. Kalender, "Validation of a Monte Carlo tool for patient-specific dose simulations in multislice computed tomography," Europ. Radiol. **18**, 759–772 (2008).
[28]D. J. Long, C. Lee, C. Tien, R. Fisher, M. R. Hoerner, D. Hintenlang, and W. E. Bolch, "Monte carlo simulations of adult and pediatric computed tomography exams: Validation studies of organ doses with physical phantoms," Med. Phys. **40**, 013901 (10pp.) (2013).
[29]G. F. Knoll, *Radiation Detection and Measurement*, 4th ed. (John Wiley and Sons, Inc., New York, 2010).
[30]S. W. S. McKeever and M. Moscovitch, "Topics under debate on the advantages and disadvantages of optically stimulated luminescence dosimetry and thermoluminescence dosimetry," Radiat. Protect. Dosim. **104**, 263–270 (2003).
[31]C. Ehringfeld, S. Schmid, K. Poljanc, C. Kirisits, H. Aiginger, and D. Georg, "Application of commercial mosfet detectors for in vivo dosimetry in the therapeutic x-ray range from 80 kv to 250 kv," Phys. Med. Biol. **50**, 289–303 (2005).
[32]A. K. Jones, F. D. Pazik, D. E. Hintenlang, and W. E. Bolch, "Mosfet dosimeter depth-dose measurements in heterogeneous tissue-equivalent phantoms at diagnostic x-ray energies," Med. Phys. **32**, 3209–3213 (2005).
[33]D. Zhang, J. DeMarco, C. Cagnon, A. Turner, M. Khatonabadi, and M. McNitt-Gray, "TH-A-214-08: Change in x-ray CT spectra inside of dosimetry phantoms: Beam hardening or beam softening?" Med. Phys. **38**, 3844 (2011).
[34]R. M. Al-Senan and M. R. Hatab, "Characteristics of an OSLD in the diagnostic energy range," Med. Phys. **38**, 4396–4405 (2011).
[35]K. R. Gorny, S. L. Leitzen, M. R. Bruesewitz, J. M. Kofler, N. J. Hangiandreou, and C. H. McCollough, "The calibration of experimental self-developing Gafchromic HXR film for the measurement of radiation dose in computed tomography," Med. Phys. **32**, 1010–1016 (2005).
[36]T. Griglock, M. Arreola, L. Sinclair, S. Bidari, and L. Gravelle, "Direct measurement of organ doses resulting from computed tomography using a cadaveric subject," paper presented at Radiological Society of North America, Scientific Assembly and Annual Meeting, November 27–December 2, Chicago IL, 2011.
[37]D. Long, E. Stepusin, L. Sinclair, and W. Bolch, "Monte Carlo patient dosimetry for computed tomography examinations with automatic tube current modulation using precalculated organ dose databases," paper presented at Radiological Society of North America, Scientific Assembly and Annual Meeting, December 1–6, Chicago IL, 2013.
[38]M. Khatonabadi, J. Mueller, K. McMillan, M. Zankl, D. Cody, C. Cagnon, J. Demarco, and M. McNitt-Gray, "Validation of Monte Carlo simulation dosimetry method using in vivo measurements in patients undergoing CT examinations," paper presented at Radiological Society of North America, Scientific Assembly and Annual Meeting, December 1–6, Chicago IL, 2013.
[39]AAPM Task Group 51, *AAPMs TG-51 Protocol for Clinical Reference Dosimetry of High-Energy Photon and Electron Beams* (American Association of Physicists in Medicine, College Park, MD, 1999).
[40]D. Zhang, X. Li, Y. Gao, X. G. Xu, and B. Liu, "A method to acquire CT organ dose map using OSL dosimeters and ATOM anthropomorphic phantoms," Med. Phys. **40**, 081918 (9pp.) (2013).
[41]J. Hsieh, *Computed Tomography: Principles, Design, Artifacts, and Recent Advances*, 2nd ed. (SPIE Press, Bellingham, WA, 2009).
[42]National Council on Radiation Protection and Measurements, *Structural Shielding Design for Medical X-Ray Imaging Facilities, NCRP Report No. 147* (NCRP, Bethesda, MD, 2005).
[43]D. Zhang, A. S. Savandi, J. J. Demarco, C. H. Cagnon, E. Angel, A. C. Turner, D. D. Cody, D. M. Stevens, A. N. Primak, C. H. McCollough, and M. F. McNitt-Gray, "Variability of surface and center position radiation dose in MDCT: Monte carlo simulations using CTDI and anthropomorphic phantoms," Med. Phys. **36**, 1025–1038 (2009).
[44]X. Li, E. Samei, C. H. Williams, W. P. Segars, D. J. Tward, M. I. Miller, J. T. Ratnanather, E. K. Paulson, and D. P. Frush, "Effects of protocol and obesity on dose conversion factors in adult body CT," Med. Phys. **39**, 6550–6571 (2012).
[45]X. G. Xu, T. Liu, L. Su, X. Du, M. Riblett, W. Ji, and F. B. Brown, "An update of ARCHER: A Monte Carlo radiation transport software testbed for emerging hardware such as GPUs," Trans. Am. Nucl. Soc. **108**, 433–434 (2013).